Solid-State ^{91}Zr NMR of Bis(cyclopentadienyl)dichlorozirconium(IV)

Ivan Hung and Robert W. Schurko*

Department of Chemistry and Biochemistry, University of Windsor, Windsor, Ontario, Canada N9B 3P4

Received: March 31, 2004

The first solid-state ^{91}Zr NMR spectra of an organometallic zirconium complex, bis(cyclopentadienyl)-dichlorozirconium(IV) (Cp_2ZrCl_2), are presented. Overlapping static and magic-angle spinning (MAS) ^{91}Zr NMR spectra of Cp_2ZrCl_2 and a zirconium oxide NMR rotor are presented to explore the possibility of conducting ^{91}Zr NMR experiments using standard ZrO_2 rotors. Quadrupolar Carr−Purcell Meiboom−Gill (QCPMG) ^{91}Zr NMR experiments on static and MAS samples, in combination with analytical and numerical spectral simulations, are used to extract ^{91}Zr quadrupolar coupling constants and asymmetry parameters. The first example of zirconium chemical shielding anisotropy is reported for Cp_2ZrCl_2, with a span of $\Omega = 475(45)$ ppm and a skew of $-0.55(5)$ (i.e., $\delta_{11} = 306$ ppm, $\delta_{22} = -62$ ppm, and $\delta_{33} = -169$ ppm). Comparison of conventional static and MAS ^{91}Zr Hahn echo NMR spectra with those acquired using the recently reported double frequency sweep/QCPMG and rotor-assisted population transfer/QCPMG pulse sequences demonstrate an order of magnitude gain in sensitivity for Cp_2ZrCl_2. Restricted Hartree−Fock and hybrid density functional theory calculations reveal that anisotropic zirconium chemical shielding tensors can be calculated with good accuracy using non-relativistic theory with large all-electron basis sets. The ^{91}Zr quadrupolar parameters for Cp_2ZrCl_2 are $C_Q = 6.35(10)$ MHz and $\eta_Q = 0.3(1)$. Reasonable agreement is obtained between calculated ^{91}Zr electric field gradient tensors and experimental results.

Introduction

There are relatively few examples of solid-state ^{91}Zr NMR in the literature due to the fact that ^{91}Zr is a half-integer quadrupolar nucleus with a moderately sized nuclear quadrupole moment (nuclear spin $I = 5/2$, $Q = -1.76(3) \times 10^{-29}$ m^2),[1] and is relatively unreceptive due to its low natural abundance (11.23%) and low magnetogyric ratio ($\gamma = -2.49750 \times 10^7$ rad T^{-1} s^{-1}). Solid-state ^{91}Zr NMR studies have previously been conducted on a number of zirconium-containing inorganic materials and metallic alloys, including Zr−Nb−Fe Laves-phase compounds,[2] zircon ($ZrSiO_4$),[3] zirconium oxide ceramics,[4,5] synthetic zirconium oxide materials,[6] sodium zirconate (Na_2ZrO_3),[7] crystalline $Na_2O-ZrO_2-SiO_2$ materials,[8] and aluminum−zirconium intermetallic alloys.[9] To the best of our knowledge, there are no reported solid-state ^{91}Zr NMR studies on organometallic zirconium complexes, although a number of different organometallic complexes have been studied in detail by solution ^{91}Zr NMR[10−12] and ab initio calculations.[11]

The majority of the aforementioned solid-state ^{91}Zr NMR studies have utilized Hahn spin-echo pulse sequences of the form $\{\pi/2-\tau-\pi-\tau-\text{acq}\}$.[13] Spin-echo sequences are required in most cases to observe the quickly decaying signal of a half-integer quadrupolar nucleus, since Bloch decay acquisition is limited by both the dead time of the coil in the NMR probe and acoustic ringing at low Larmor frequencies. Due to both the broadening of solid-state NMR powder patterns by the second-order quadrupolar interaction and the generally poor receptivity of ^{91}Zr, many of these spectra require the acquisition of hundreds of thousands of transients to obtain a reasonable signal-to-noise (S/N) ratio. Further, if the ^{91}Zr quadrupolar interaction is large, the breadth of the ^{91}Zr spectrum exceeds excitation bandwidths at standard magnetic field strengths (i.e., 9.4−14.1 T); thus, in some cases it is necessary to collect spectra that are 50−600 kHz wide in a stepwise manner (in frequency offset increments), which is a very time-consuming process.[14,15] In addition, many of the spectra acquired by stepped-echo techniques lack the definition (i.e., S/N ratio and spectral resolution) required to obtain accurate chemical shielding and quadrupolar parameters from spectral analysis.

There has recently been much progress in the observation of unreceptive low-γ half-integer quadrupolar nuclei owing to the availability of higher magnetic fields and stable low-temperature double-resonance NMR probes and the development of special spin-echo pulse sequences.[16,17] In particular, a multiple-pulse spin-echo technique for quadrupolar nuclei, known as the "quadrupolar Carr−Purcell Meiboom−Gill" (QCPMG) pulse sequence,[18] has found application in the study of dilute, insensitive quadrupolar nuclei in inorganic materials[19] and biologically relevant samples.[20,21] QCPMG has also been modified for magic-angle spinning (MAS) and multiple-quantum magic-angle spinning (MQMAS) to study receptive half-integer quadrupolar nuclei with large quadrupolar interactions.[22,23] In addition, the QCPMG pulse sequence has recently been combined with the preparatory rotor-assisted population transfer (RAPT)[24] and amplitude-modulated double frequency sweep (AM-DFS)[25] pulse sequences for overall signal enhancements of an order of magnitude or more.[26]

The first solid-state ^{91}Zr NMR study of an organometallic zirconium(IV) complex using Hahn echo, QCPMG, and modified QCPMG pulse sequences is presented. The compound under investigation is bis(cyclopentadienyl)dichlorozirconium(IV) (Cp_2ZrCl_2), which is an important precursor in the design of zirconium containing metallocene catalysts.[27] Acquisition of static and MAS ^{91}Zr QCPMG NMR spectra of Cp_2ZrCl_2 packed in a zirconium oxide NMR rotor shows that there is some degree

* To whom correspondence should be addressed. Fax: (519) 973-7098. E-mail: rschurko@uwindsor.ca.

10.1021/jp040270u CCC: $27.50
Published on Web 05/29/2004

SCHEME 1

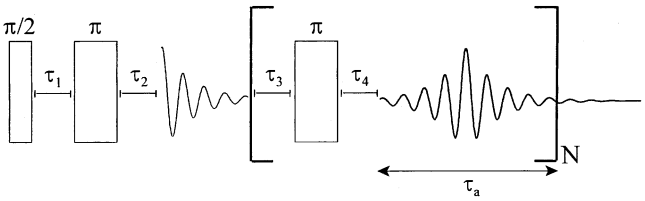

of background signal from the rotor, but it can be easily distinguished from the Cp_2ZrCl_2 signal. It is demonstrated that ZrO_2 rotors are suitable for MAS NMR experiments on compounds with small to moderate quadrupole coupling constants such as Cp_2ZrCl_2, and that Zr-free sample containers are a necessity for Zr compounds with larger quadrupolar interactions. The central transition ^{91}Zr NMR spectra, which are influenced by anisotropic chemical shielding and second-order quadrupolar effects, can be used to probe the electronic environment about the zirconium atom. The first anisotropic zirconium chemical shielding tensor is determined from simulation of experimental ^{91}Zr static spectra acquired at two different field strengths. Significant gains in signal can be obtained in the ^{91}Zr NMR spectra of Cp_2ZrCl_2 by using preparatory DFS or RAPT sequences, followed by the QCPMG sequence. Our work demonstrates that it is possible to rapidly and efficiently acquire solid-state ^{91}Zr NMR spectra of zirconium-containing organometallic and inorganic materials using QCPMG methods, regardless of the magnitude of the quadrupolar interaction. These techniques hold promise for the investigation of catalytic mechanisms in solid zirconium-containing systems, in addition to a wide array of technologically important materials. We also present various theoretical calculations of NMR interaction tensors, for the purpose of examining the orientations of the NMR interaction tensors within the molecular frame and correlating the anisotropic NMR interactions to the molecular structure.

Experimental Section

Cp_2ZrCl_2 was purchased from Strem Chemicals, Inc. and used without further purification.

Solid-State NMR Spectroscopy. Zirconium-91 NMR spectra were acquired on a Varian Infinity Plus NMR spectrometer with an Oxford $B_0 = 9.4$ T ($\upsilon_0(^1H) = 400$ MHz) wide-bore magnet operating at $\upsilon_0(^{91}Zr) = 37.16$ MHz. Samples were finely powdered and packed under a nitrogen atmosphere into a 4 mm o.d. zirconia rotor for MAS experiments, and into both a 5 mm o.d. zirconia rotor and a 5 mm o.d. Teflon tube for static experiments. All ^{91}Zr experiments employed a central transition selective $\pi/2$ pulse width of 1.17 μs, rf field υ_1 of 71.4 kHz, and recycle delay of 0.75 s. Static QCPMG spectra of Cp_2ZrCl_2 packed in a Teflon tube were recorded using interpulse and interacquisition delays $\tau_1 = \tau_2 = \tau_3 = \tau_4 = 45$ μs to minimize the effects of probe ringing (see Scheme 1). The acquisition period (τ_a) for each echo was adjusted to attain a spikelet separation ($1/\tau_a$) of 1905 Hz in the frequency spectrum, and the number of Meiboom−Gill (MG) loops was set to acquire the complete transverse decay of the free induction decay (FID). Where applicable, a converging DFS pulse was employed starting at $\upsilon_s = 2$ MHz and finishing at $\upsilon_f = 185$ kHz over a period of 800 μs, which corresponds to a sweep rate (λ) of ca. 2.3 GHz s^{-1} and an adiabaticity parameter ($A = \upsilon_1^2/\lambda$) of 2.25.[28] The static QCPMG subspectra of Cp_2ZrCl_2 in a 5 mm o.d. zirconia rotor and a rotor containing an adamantane/KBr mixture (i.e., to measure the ^{91}Zr background from the rotor) were acquired in a stepwise fashion using 50 kHz irradiation frequency offsets (integer multiple of $1/\tau_a$) until no signal could be detected upon further increase or decrease of the transmitter frequency. Uniform excitation over a "rectangular" spectral region was accomplished by determining the effective excitation bandwidth for given rf fields and pulse widths from an individual sub-spectrum and then setting the appropriate transmitter offset step size (which is also a multiple of spikelet separation).[29−31] For each subspectrum 3200 transients were collected with $1/\tau_a = 2000$ Hz and $\tau_1 = \tau_2 = \tau_3 = \tau_4 = 35$ μs. Central transition selective pulse widths mentioned herein are non-selective pulse widths which have been scaled by the factor $(I + {}^1/_2)^{-1}$. Zirconium-91 chemical shifts were referenced to a concentrated solution of Cp_2ZrCl_2 in CH_2Cl_2 ($\delta_{iso} = 0$ ppm).

All MAS experiments were synchronized with the rotor period by setting τ_1 equal to the inverse of the rotor spinning frequency, υ_{rot}, or a multiple thereof. Since all MAS experiments were performed at $\upsilon_{rot} = 15$ kHz, all τ_1 values were set to either 66.67 or 133.34 μs; MAS Hahn echo experiments employed $\tau_1 = 133.34$ μs and $\tau_2 = 70.84$ μs. For the ^{91}Zr MAS QCPMG spectrum, 14642 transients were acquired with 40 MG loops, $\tau_a = 2$ ms, and $\tau_1 = \tau_2 = 66.67$ μs, while τ_3 and τ_4 were set to 65.5 μs according to the equation $2N\tau_r = \tau_a + \tau_3 + \tau_4 + \tau_\pi$, where N is an integer, τ_r is the rotor period, $\tau_3 = \tau_4$, and τ_π is the duration of the selective π pulse.[22] The recently reported RAPT sequence for spin 5/2 nuclei was employed,[32] where two consecutive RAPT sequences are involved: the former utilized an $X-\bar{X}$ unit of 2.02 μs repeated 37 times and the latter an $X-\bar{X}$ unit of 2.4 μs repeated 48 times; a subsequent delay of 1.5 μs was instilled before the $\pi/2$ pulse.

For the comparison of RAPT- and DFS-enhanced spectra with conventional spectra, a total of 8000 transients were collected for all non-spinning ^{91}Zr NMR spectra and MAS spin-echo spectra, while 800 scans were collected for MAS QCPMG type experiments. The same parameters (including those for DFS and RAPT) were employed for spectra in this section as those mentioned above, except τ_a was set to 512 μs and 1 ms for static and MAS QCPMG spectra, respectively. For further background information on the combination of DFS and RAPT sequences with QCPMG pulse trains, we refer the reader to ref 26.

In addition, a static Hahn echo spectrum of Cp_2ZrCl_2 packed into a 4 mm o.d. Teflon tube was acquired on a Bruker DRX-500 NMR spectrometer (usually dedicated to solution NMR) with a 11.74 T ($\upsilon_0(^1H) = 500$ MHz) standard-bore magnet operating at $\upsilon_0(^{91}Zr) = 46.5$ MHz to aid in the extraction of ^{91}Zr chemical shielding tensor parameters. A standard-bore double-resonance HX NMR probe with a Helmholz coil was used for all experiments on the DRX-500. For experiments conducted at $B_0 = 11.74$ T, a $\pi/2$ pulse width of 6 μs, rf field $\upsilon_1 = 13.9$ kHz, and spectral width of 100 kHz were employed with τ_1 and τ_2 set to 150 and 40 μs, respectively.

Spectral Simulations. Analytical simulations of ^{91}Zr static and MAS NMR spectra were generated with the WSOLIDS software package written and developed by K. Eichele in R. E. Wasylishen's laboratory at Dalhousie University. Further refinement of these parameters was obtained via numerical simulations of QCPMG spectra with the SIMPSON software package.[33] SIMPSON simulations were accomplished by the *direct* method of powder averaging using 20 γ angles and the zcw4180 crystal file provided with the package. The start and detect operators were set to I_{1z} and I_{1c}, respectively, while all other parameters, including the interpulse acquisition period ($1/\tau_a$), central transition selective pulse widths, and interpulse delays, were set equal

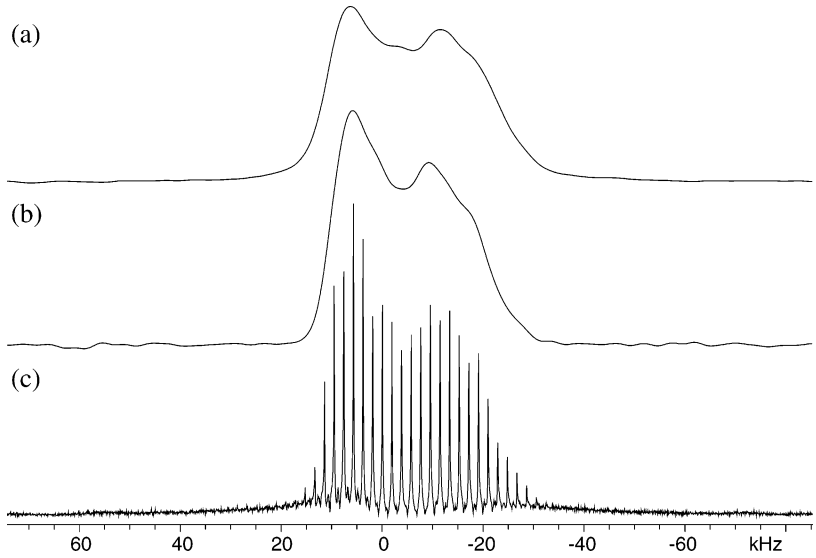

Figure 1. ^{91}Zr static NMR spectra of Cp_2ZrCl_2: (a) DFS/Hahn echo spectrum (1925 min acquisition time), (b) DFS/QCPMG spectrum, from Fourier transformation of co-added echoes, and (c) DFS/QCPMG spectrum, from Fourier transformation of the complete echo train (197 min acquisition time).

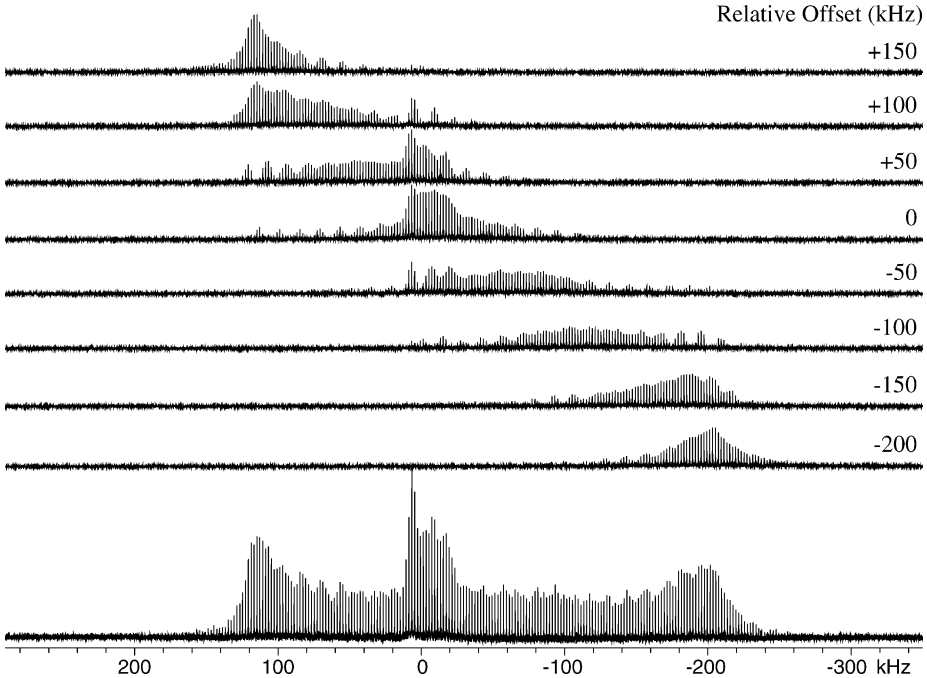

Figure 2. Piecewise acquisition of the static ^{91}Zr QCPMG NMR spectrum of Cp_2ZrCl_2 packed inside a 5 mm o.d. ZrO_2 rotor. Irradiation frequencies are offset by 50 kHz steps to acquire the complete powder pattern.

to those employed experimentally. Simulated spectra were saved in ASCII format as FID files without any mathematical manipulation and converted to files readable by the NUTS (Acorn NMR) software for further processing. Best-fit spectra were obtained by comparison of root-mean-square difference spectra, and error bounds were determined through bidirectional variation of the NMR parameters.

Conventions used for the specification of electric field gradient (EFG) and chemical shift parameters differ between the WSOLIDS and SIMPSON simulation programs, and the reader is alerted to these differences. Whereas WSOLIDS uses the right-handed EFG and chemical shift tensors given by ($|V_{zz}| \geq |V_{yy}| \geq |V_{xx}|$; $C_Q = eV_{zz}Q/h$; $\eta_Q = (V_{xx} - V_{yy})/V_{zz}$) and ($\delta_{11} \geq \delta_{22} \geq \delta_{33}$; $\Omega = \delta_{11} - \delta_{33}$; $\kappa = 3(\delta_{22} - \delta_{iso})/\Omega$), respectively, the conventions employed in SIMPSON differ ($|V_{zz}| \geq |V_{xx}| \geq |V_{yy}|$; $C_Q = eV_{zz}Q/h$; $\eta_Q = (V_{yy} - V_{xx})/V_{zz}$; $|\delta_{zz} - \delta_{iso}| \geq |\delta_{xx} - \delta_{iso}| \geq |\delta_{yy} - \delta_{iso}|$; $\delta = \delta_{zz} - \delta_{iso}$; $\kappa = (\delta_{yy} - \delta_{xx})/\delta$). In cases where the chemical shift and EFG tensors do not coincide, Euler angles are implemented to describe their relative orientation. One must be cautious in selecting Euler angles appropriate to the convention implemented within the simulation software. The WSOLIDS conventions are followed in the present work. Namely, the Euler angles α, β, and γ are employed for unitary transformations in the order $\mathbf{R}_{z''}(\gamma)$ $\mathbf{R}_{y'}(\beta)$ $\mathbf{R}_z(\alpha)$,[34,35] where $\mathbf{R}_i(\theta)$ performs a counterclockwise (positive) rotation about the positive i-axis by angle θ, producing a new rotation axis i', such that a coordinate system initially coincident with the EFG principal axis system (PAS) ends up coincident with the chemical shift PAS after the transformation (i.e., an active transformation).

Theoretical Calculations. Calculations of EFG and chemical shielding (CS) tensors were performed using Gaussian 98[36] on

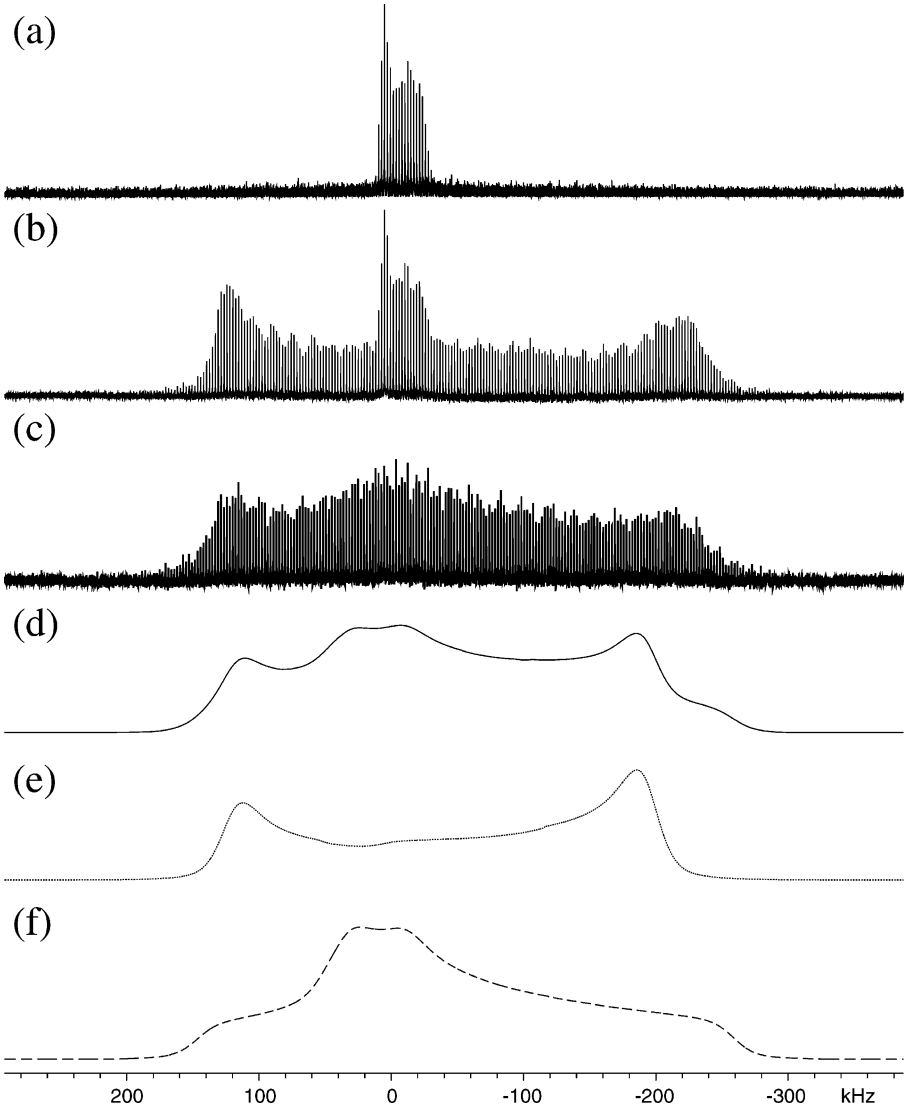

Figure 3. Static ^{91}Zr QCPMG NMR spectra of Cp_2ZrCl_2 packed inside (a) a 5 mm o.d. Teflon tube and (b) a 5 mm o.d. ZrO_2 rotor and (c) ^{91}Zr QCPMG spectrum of a ZrO_2 rotor filled with adamantane and KBr (this latter sample is to get a measurement of the ^{91}Zr NMR spectrum arising solely from the rotor). Simulated static ^{91}Zr NMR powder patterns for (d) a 7:10 mixture of tetragonal and orthorhombic phases of zirconia, along with the subspectra for (e) the tetragonal phase ($C_Q = 19.4$ MHz, $\eta_Q = 0.0$, $\delta_{iso} = 200$ ppm) and (f) the orthorhombic phase ($C_Q = 16.5$ MHz, $\eta_Q = 0.85$, $\delta_{iso} = 300$ ppm) of zirconia.

a Dell Precision 420 workstation with dual 733 MHz Pentium III processors running Red Hat Linux 6.2. Molecular coordinates of Cp_2ZrCl_2 used in calculations were obtained from crystal structure data resolved by X-ray diffraction.[37] Calculations of NMR interaction tensors of the fully optimized gas-phase geometry were also performed (see the Supporting Information), and poorer agreement with experimental data was obtained. Computations were carried out using restricted Hartree−Fock (RHF) and hybrid density functional theory (DFT) with the B3LYP functional.[38−40] The 6-31G** and 6-311G** basis sets were used for all nuclei except zirconium, for which expanded all-electron basis sets were applied [3F (33333/333/33), 3F (43222/422/33), 3F (43333/433/43), 5F (33333/333/33), 5F (43222/422/33), and 5F (43333/433/43), designated, respectively, as 3F1, 3F2, 3F3, 5F1, 5F2, and 5F3].[41] Zirconium 3F and 5F basis sets differ in the occupation of the valence orbitals: 3F and 5F represent the KLM$4s^2 4p^6 4d^2 5s^2$ and KLM$4s^2 4p^6 4d^3 5s^1$ ground-state configurations, respectively. Chemical shielding tensors were calculated using the GIAO method[42,43] without taking relativistic effects into account. Calculated shielding data were referenced by setting the theoretical isotropic chemical shielding of Cp_2ZrCl_2 to $\delta_{iso} = 0.0$ ppm.

Results and Discussion

Solid-State ^{91}Zr NMR. Comparison of ^{91}Zr DFS/Hahn echo and DFS/QCPMG NMR spectra of Cp_2ZrCl_2 (Figure 1) in a stationary Teflon sample tube reveals that the QCPMG powder pattern is split into "spikelets" and possesses a significant signal enhancement. The acquisition times of the ^{91}Zr DFS/Hahn echo (Figure 1a) and DFS/QCPMG NMR (Figure 1b,c) spectra were approximately 1925 and 197 min, respectively. The integrated intensity of a QCPMG spectrum can be compared to that of a standard spin-echo spectrum by co-adding the echoes in the time domain and then performing a Fourier transform (Figure 1b) followed by powder pattern integration. Alternatively, one may also compare the signal-to-noise ratio between the spikelet form of the QCPMG spectrum (Figure 1c) and the conventional Hahn echo spectrum, though variability in the properties of echo and QCPMG spectra make accurate numerical comparisons dubious. The co-added echo spectrum has an integrated intensity of 1.1

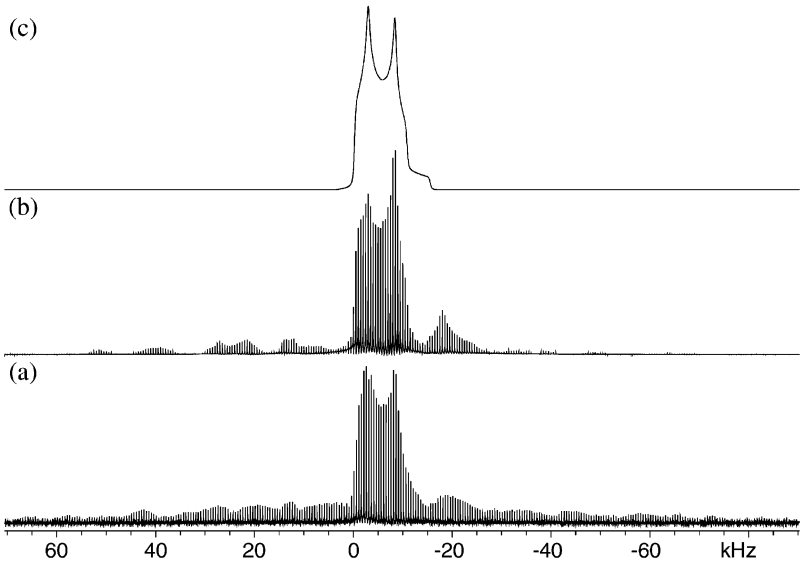

Figure 4. (a) Experimental ^{91}Zr MAS RAPT/QCPMG NMR spectrum of Cp_2ZrCl_2 along with (b) numerical (SIMPSON) and (c) analytical (WSOLIDS) simulations.

compared to the normalized intensity of the echo spectrum (which is set to 1.0), and a higher signal-to-noise ratio, despite the fact that 10 times fewer scans are acquired in the DFS/QCPMG experiment. The signal-to-noise ratio gain in the spectrum obtained using the QCPMG pulse sequence arises from localization of intensity under sharp spikelets resulting from the repetitive collection of *numerous* spin echoes within a single acquisition and subsequent Fourier transformation. The extent to which spin echoes can be acquired depends on the T_2 relaxation time constant specific to the nuclei in the sample. The magnitude of signal-to-noise ratio enhancement also depends on the spacing of spin echoes in the time domain, and consequently, on the separation of the spikelets in the frequency domain after Fourier transformation of the FID. It is necessary to adjust $1/\tau_a$ to attain the optimum signal intensity and S/N ratio enhancement while retaining sufficient resolution to extract the desired NMR parameters. Comparison of the spectra in Figure 1 demonstrates that NMR parameters extractable from the conventional Hahn echo experiment can very well be obtained from the envelope of a closely spaced QCPMG spectrum.

Static ^{91}Zr QCPMG NMR experiments on Cp_2ZrCl_2 in a standard 5 mm o.d. NMR rotor reveal a powder pattern similar to what is acquired for the sample in a Teflon tube. However, the spectrum is not as well-defined and displays portions of another broad powder pattern flanking the expected pattern. This additional powder pattern, which is characteristic of a very large quadrupolar coupling constant, arises from ^{91}Zr nuclei in the rotor. A stepped-echo experiment (see the Experimental Section for details) combined with QCPMG (Figure 2) was employed to record the full breadth of the ^{91}Zr powder pattern.[44] The individually acquired segments were Fourier transformed and summed together to produce the full powder pattern (see the Supporting Information for a comparison with the wide-line spectrum resulting from a skyline projection of the individual pieces).

A comparison of the ^{91}Zr QCPMG NMR spectra of Cp_2ZrCl_2 in the ZrO_2 rotor and in the Teflon sample tube, as well as a ZrO_2 rotor containing an adamantane/KBr mixture, is shown in Figure 3. Clearly, the background interference from the ^{91}Zr nuclei in the rotor is substantial enough to warrant the use of a zirconium-free sample container or rotor for static NMR experiments, since accurate simulation of the ^{91}Zr powder pattern is complicated by the presence of the broad underlying powder pattern. A simulation of ^{91}Zr powder patterns corresponding to a mixture of tetragonal and orthorhombic phases of zirconia (in ca. 7:10 ratio) roughly approximates the shape of the rotor powder pattern. Simulations of the individual ^{91}Zr NMR powder patterns for the tetragonal and orthorhombic phases are based on data for disordered zirconium oxide materials previously reported by Bastow and co-workers,[14] and neglect any effects of chemical shielding anisotropy.

It is of interest to determine whether ZrO_2 rotors can be used for ^{91}Zr MAS NMR experiments, since they are the most reliable and readily available ceramic rotors currently used. An experimental ^{91}Zr MAS RAPT/QCPMG NMR spectrum acquired at $\upsilon_{rot} = 15$ kHz (Figure 4a) displays a single second-order quadrupolar pattern at $\delta_{iso} = 25(15)$ ppm. The difference in isotropic shifts between powdered Cp_2ZrCl_2 and the same sample dissolved in CH_2Cl_2 (i.e., $\delta_{iso} = 0.0$ ppm) can be attributed to solvent effects and/or crystal packing. The SIMPSON and MAS envelope simulations (Figure 4b,c) yield $C_Q = 6.35(10)$ MHz, which is comparable to some of the relatively smaller $C_Q(^{91}Zr)$ values measured previously by Hartmann and Scheler in various zirconates,[15] and $\eta_Q = 0.3(1)$. There are actually two distinct Cp_2ZrCl_2 molecules in the unit cell with magnetically non-equivalent ^{91}Zr nuclei;[37] however, their structures are alike, and the values of C_Q, η_Q, and δ_{iso} are expected to be very similar. This is evidenced by the observation of a single type of ^{91}Zr environment as well as ab initio calculations of ^{91}Zr NMR interaction tensors (see the discussion of ab initio data below as well as the Supporting Information). The QCPMG pulse sequence gives rise to spectra in the form of spikelets which are offset from the irradiation frequency by $1/\tau_a$; therefore, differentiation of nonequivalent sites by chemical shift is not possible unless gross differences (i.e., fairly distinct overlapping powder patterns) can be observed. Numerical simulations of the ^{91}Zr MAS QCPMG NMR spectrum of the ZrO_2 rotor were also conducted (not shown), revealing a complicated powder pattern composed of overlapping isotropic and spinning sidebands. The intensity of this spectrum is very low due to the comparatively large value of $C_Q(^{91}Zr)$ in ZrO_2 and does not significantly interfere with the spectrum of Cp_2ZrCl_2. Nonetheless, a small influence on

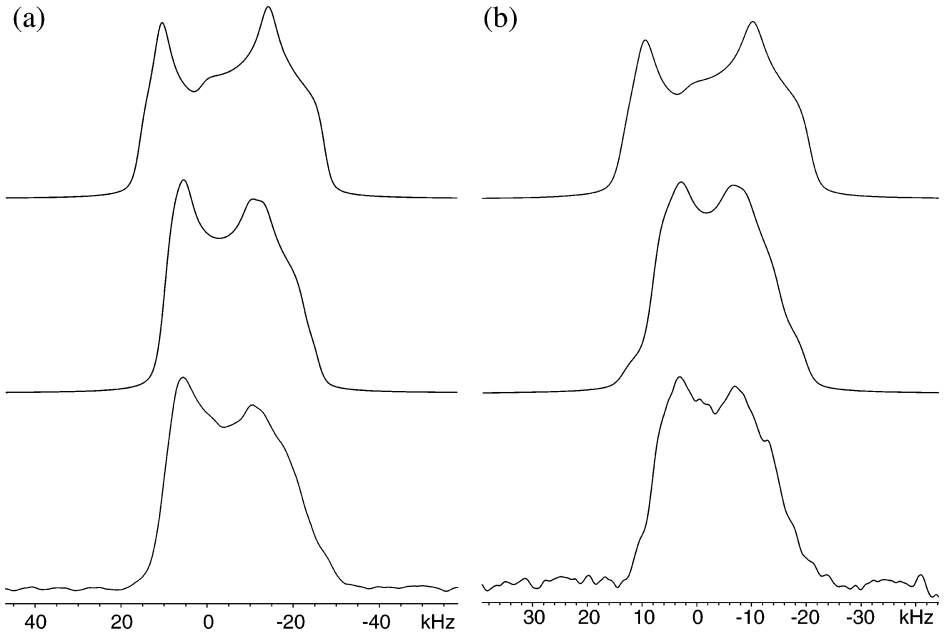

Figure 5. Experimental (bottom trace) ^{91}Zr static NMR spectra of Cp_2ZrCl_2 along with simulations including (middle trace) and excluding (top trace) the effects of CSA at magnetic fields (a) $B_0 = 9.4$ T and (b) $B_0 = 11.74$ T.

TABLE 1: Experimental Zirconium-91 Chemical Shift and Quadrupolar Parameters

parameter	Cp_2ZrCl_2		ZrO_2 rotor
magnetic field, B_0 (T)	9.4	11.74	9.4
C_Q (MHz)	6.35(10)	6.35(10)	19.9(6)
η_Q[a]	0.3(1)	0.3(1)	0.04(2)
δ_{iso}[b] (ppm)	25	40	60(30)
κ[d]	−0.55	−0.50	
δ_{11}[e] (ppm)	306	291	
δ_{22} (ppm)	−62	−32	
δ_{33} (ppm)	−169	−139	
α[f] (deg)	26	31	
β (deg)	92	89	
γ (deg)	10	11	
Ω[c] (ppm)	475	430	

[a] Quadrupolar asymmetry parameter, $\eta_Q = (V_{11} - V_{22})/V_{33}$. [b] Isotropic shift, $\delta_{iso} = (\delta_{11} + \delta_{22} + \delta_{33})/3$. [c] Span of the CS tensor, $\Omega = \delta_{11} - \delta_{33}$. [d] Asymmetry of the CS tensor, $\kappa = 3(\delta_{22} - \delta_{iso})/\Omega$. [e] Principal components of the CS tensor from least to most shielded: $\delta_{11} \geq \delta_{22} \geq \delta_{33}$. [f] Euler angles α, β, and γ for rotation of the CS principal axis system into the EFG principal axis system.

the ^{91}Zr MAS QCPMG NMR spectrum of Cp_2ZrCl_2 is observed, being especially pronounced in regions between the spinning sidebands where "extra intensity" can be seen (Figure 4a).

Simulation of the Cp_2ZrCl_2 static ^{91}Zr NMR powder patterns acquired at magnetic fields of 9.4 T (Figure 5a, bottom trace) and 11.74 T (Figure 5b, bottom trace) reveal the presence of zirconium chemical shielding anisotropy (CSA). Spectral simulations employing only quadrupolar parameters and the isotropic chemical shift (obtained from analysis of MAS QCPMG NMR spectra) excluding the effects of CSA (Figure 5, top traces) yield patterns which do not match the appearance of experimentally recorded spectra. Simulations including CSA (Figure 5, middle traces) point to a non-axial chemical shielding tensor with parameters $\delta_{iso} = 25(15)$ ppm, $\Omega = 475(45)$ ppm, and $\kappa = -0.55(5)$, corresponding to the principal components $\delta_{11} = 306$ ppm, $\delta_{22} = -62$ ppm, and $\delta_{33} = -169$ ppm. CSA parameters corresponding to spectra acquired at a lower field ($B_0 = 9.4$ T) are taken as the primary values for discussion (Table 1) due to the higher S/N ratio in these spectra resulting from larger sample volume and higher rf field. To the best of our knowledge, this is the only report of zirconium chemical shielding anisotropy to date. Due to the presence of relatively large quadrupole couplings in many zirconium compounds, it is often not possible to establish the presence of chemical shielding anisotropy without the use of two or more vastly different magnetic fields, unless its effects are quite pronounced. Even in the case presented here, the contribution of the second-order quadrupolar interaction to the overall breadth of the ^{91}Zr powder pattern of Cp_2ZrCl_2 is considerably larger than that of the chemical shielding anisotropy, and a high degree of accuracy cannot be attained in the extraction of Zr CSA.

Simulations of the experimental static spectra reveal that the zirconium CS and EFG tensors are not coincident; it is well-known that the relative orientations of the CS and EFG tensors can have dramatic effects on the appearance of solid-state NMR powder patterns of half-integer quadrupolar nuclei.[45−47] For Cp_2ZrCl_2, the Euler angles describing the orientation of the CS tensor with respect to the EFG tensor are $\alpha = 26(5)°$, $\beta = 92(3)°$, and $\gamma = 10(1)°$. The relationships between these Euler angles and the orientation of the CS and EFG tensors with respect to the molecular frame are discussed later in this paper.

Signal Enhancement Pulse Techniques. The use of amplitude-modulated DFSs for signal enhancement of the central transition by population inversion (e.g., of the $\pm 1/2$ and $\pm 3/2$ levels of spin 3/2 nuclei) has been known for approximately a decade.[28,48] In particular, it has been found that setting an adequate DFS rate and finishing frequency (υ_f) is of paramount importance for sweeps to be effective. An adiabaticity parameter, A, is often quoted to characterize the efficiency of the DFS population inversion.[25] Another scheme for signal enhancement of the central transition, RAPT, which takes advantage of population transfer during sample spinning, has also been developed.[24,49] The RAPT pulse sequence saturates all the nuclear spin levels of the same sign, yielding a theoretical signal enhancement of $I + 1/2$, where I is the nuclear spin. Both techniques mentioned above have recently been combined with QCPMG to yield an even greater enhancement in overall signal;[26] their performance is briefly examined below for the case of Cp_2ZrCl_2.

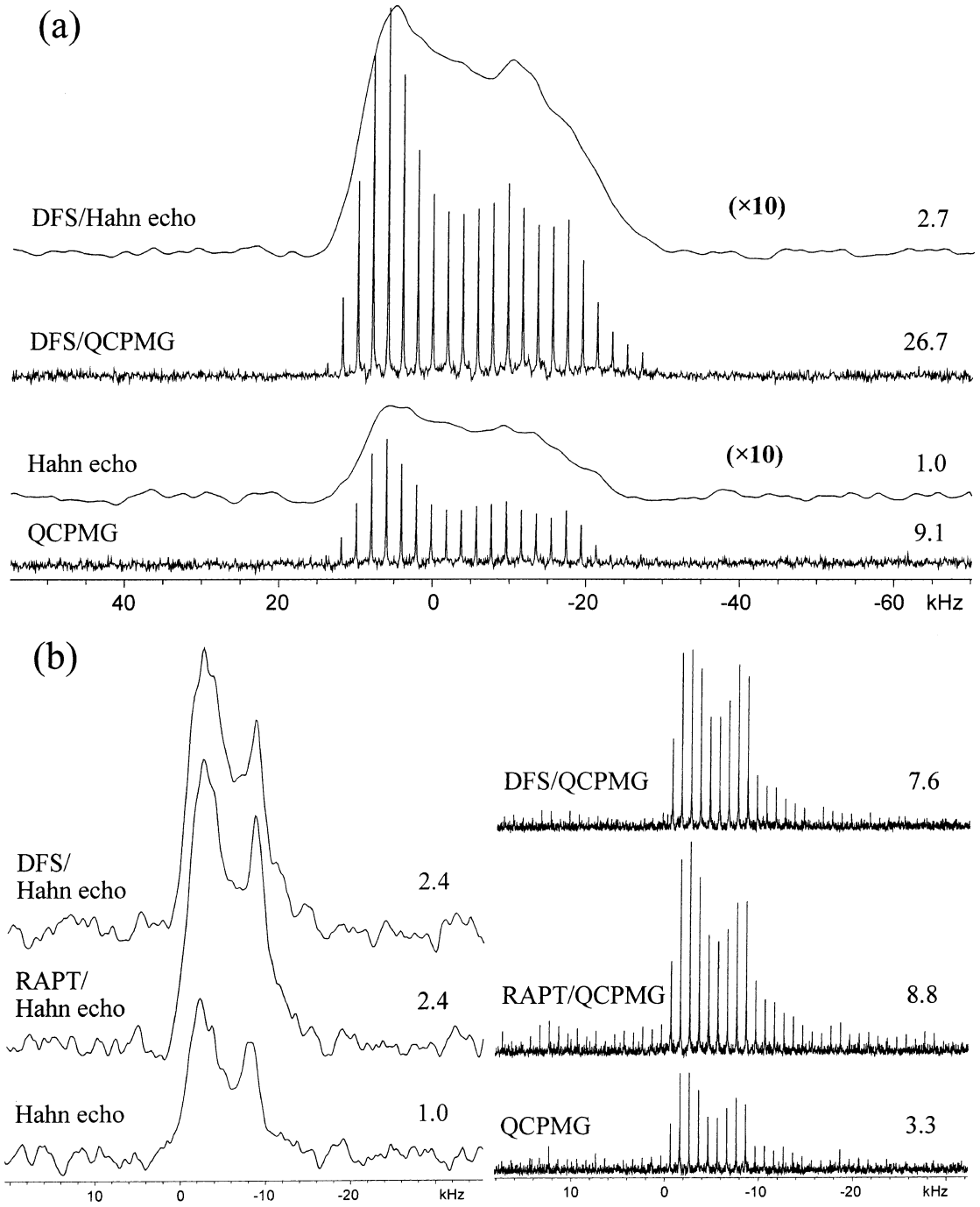

Figure 6. (a) Static ^{91}Zr Hahn echo and DFS/echo NMR spectra of Cp_2ZrCl_2 and corresponding QCPMG experiments (the same number of transients recorded in each case). The vertical scales of echo spectra are augmented by a factor of 10. (b) ^{91}Zr MAS Hahn echo, RAPT/echo, DFS/echo, and corresponding QCPMG NMR spectra of Cp_2ZrCl_2. MAS QCPMG experiments were acquired with 10 times fewer scans than their spin-echo counterparts. Integrated intensities with respect to the static and MAS ^{91}Zr Hahn echo experiments are located to the right of each spectrum.

Static ^{91}Zr Hahn echo, DFS/echo, QCPMG and DFS/QCPMG NMR spectra are shown in Figure 6a. The QCPMG pulse sequence alone increases the signal intensity 9.1 times compared to the conventional Hahn echo experiment (normalized integrated intensity of 1.0). The DFS preparatory pulse yields enhancements of 2.7 and 2.9 in integrated intensity for echo and QCPMG experiments, respectively. Overall, the DFS/QCPMG sequence provides an enhancement of 26.7 times with respect to the Hahn echo experiment. The theoretical signal enhancement achievable by DFS is 2*I*, which for the case of ^{91}Zr ($I = 5/2$) should be 5. However, due to the distribution of crystallite orientations in powder samples which results in varying magnitudes of C_Q, only an enhancement of ca. 3 is expected.[50]

^{91}Zr MAS NMR spectra are shown in Figure 6b. It is important to note that MAS QCPMG experiments were recorded with 10 times fewer transients than their echo counterparts, yet comparison of Hahn echo and QCPMG spectra shows that the latter possess 3 times greater integrated intensity! Both the RAPT and DFS preparation pulses give a signal enhancement of 2.4 compared to the Hahn echo, while enhancements of 2.7 and 2.3 are observed, respectively, for corresponding QCPMG

TABLE 2: Theoretical Zirconium Chemical Shift Tensors in Cp_2ZrCl_2[a]

source	δ_{11}[b] (ppm)	δ_{22} (ppm)	δ_{33} (ppm)	δ_{iso} (ppm)	Ω (ppm)	κ
experiment						
$B_0 = 9.4$ T	306	−62	−169	25	475	−0.55
$B_0 = 11.74$ T	291	−32	−139	40	430	−0.50
RHF/6-31G**						
3F (33333/333/33)	30.9	25.7	−56.6	0.0	87.5	0.88
3F (43222/422/33)	27.9	20.5	−48.4	0.0	76.3	0.80
3F (43333/433/43)	166.3	−33.6	−132.8	0.0	299.1	−0.34
5F (33333/333/33)	61.5	9.1	−70.5	0.0	132.0	0.21
5F (43222/422/33)	49.3	11.8	−61.0	0.0	110.3	0.32
5F (43333/433/43)	201.5	−51.1	−150.4	0.0	351.9	−0.44
RHF/6-311G**						
3F (33333/333/33)	38.3	8.8	−47.0	0.0	85.3	0.31
3F (43222/422/33)	32.8	8.2	−41.1	0.0	73.9	0.34
3F (43333/433/43)	160.0	−31.8	−128.2	0.0	288.2	−0.33
5F (33333/333/33)	20.6	20.1	−40.7	0.0	61.3	0.98
5F (43222/422/33)	26.7	16.2	−42.9	0.0	69.6	0.70
5F (43333/433/43)	204.4	−42.6	−161.8	0.0	366.1	−0.35
DFT(B3LYP)/6-31G**						
3F (33333/333/33)	94.9	2.1	−97.1	0.0	192.0	0.03
3F (43222/422/33)	81.0	5.3	−86.3	0.0	167.2	0.10
3F (43333/433/43)	236.6	−58.3	−178.3	0.0	414.9	−0.42
5F (33333/333/33)	120.2	−13.5	−106.8	0.0	227.0	−0.18
5F (43222/422/33)	105.9	−9.8	−96.2	0.0	202.1	−0.15
5F (43333/433/43)	263.3	−74.5	−188.9	0.0	452.2	−0.49
DFT(B3LYP)/6-311G**						
3F (33333/333/33)	34.5	9.0	−43.4	0.0	77.9	0.35
3F (43222/422/33)	35.1	7.1	−42.1	0.0	77.2	0.28
3F (43333/433/43)	213.1	−63.2	−149.9	0.0	363.0	−0.52
5F (33333/333/33)	59.1	−2.7	−56.4	0.0	115.5	−0.07
5F (43222/422/33)	63.8	−5.4	−58.3	0.0	122.1	−0.13
5F (43333/433/43)	246.2	−69.7	−176.5	0.0	422.8	−0.50

[a] Geometry of Cp_2ZrCl_2 taken from experimental X-ray crystal structure. Presented data are for calculations using 3F/5F basis sets on zirconium and 6-31G**/6-311G** for all other atoms. See the Experimental Section for details. [b] Absolute chemical shielding data are converted to chemical shifts with the formula $\sigma_{ref} - \sigma_{sample}$, where σ_{ref} is the absolute chemical shielding of Cp_2ZrCl_2.

experiments. The poor S/N ratio and severe distortions seen in MAS spectra are caused by the ^{91}Zr NMR signal of the rotor, which also accounts for the large amount of spikelets on the baseline surrounding the powder pattern of MAS QCPMG experiments. The combination of DFS or RAPT with QCPMG leads to spectra with considerably higher S/N ratio (or integrated intensity in the case of co-added echoes), meaning greatly reduced experimental times are possible.

Theoretical Calculations. Experimental and theoretical zirconium chemical shielding tensors are shown in Table 2, where theoretical shielding values have been converted to chemical shifts as described in the Experimental Section. Agreement between experimental and theoretical shielding tensors improves as larger zirconium basis sets (3F1 → 3F3 and 5F1 → 5F3) are employed. Changing the basis set on all of the other atoms results in significant changes in the zirconium CS tensors for many of the calculations, except those using the 3F3 and 5F3 Zr basis sets. In particular, relatively accurate calculations of the span ($\Omega = 475(45)$ ppm) and asymmetry parameter ($\kappa = -0.55(5)$) of the zirconium chemical shielding tensor only occur for calculations employing zirconium F3 basis sets, with 5F3 consistently giving the best agreement with experiment. Compared to RHF, most B3LYP calculations yield higher values of Ω and κ, and consistently afford much better agreement with experimental data.

TABLE 3: Theoretical Zirconium Quadrupolar Parameters in Cp_2ZrCl_2[a]

source	V_{11}[b] (au)	V_{22} (au)	V_{33} (au)	$\lvert C_Q\rvert$[c] (MHz)	η_Q
experiment				6.35(10)	0.3(1)
RHF/6-31G**					
3F (33333/333/33)	0.1223	0.2480	−0.3703	15.31	0.34
3F (43222/422/33)	0.0996	0.2312	−0.3308	13.68	0.40
3F (43333/433/43)	0.0695	0.1129	−0.1824	7.54	0.24
5F (33333/333/33)	0.1266	0.2171	−0.3437	14.21	0.26
5F (43222/422/33)	0.1012	0.1989	−0.3001	12.41	0.33
5F (43333/433/43)	0.0494	0.1015	−0.1509	6.24	0.34
RHF/6-311G**					
3F (33333/333/33)	0.2205	0.4953	−0.7158	29.60	0.38
3F (43222/422/33)	0.1917	0.4223	−0.6140	25.39	0.38
3F (43333/433/43)	0.0954	0.1824	−0.2778	11.49	0.31
5F (33333/333/33)	0.2080	0.4091	−0.6181	25.52	0.33
5F (43222/422/33)	0.1741	0.3292	−0.5033	20.81	0.31
5F (43333/433/43)	0.0634	0.1056	−0.1690	6.99	0.25
DFT(B3LYP)/6-31G**					
3F (33333/333/33)	0.1593	0.2995	−0.4588	18.97	0.31
3F (43222/422/33)	0.1375	0.2827	−0.4201	17.37	0.35
3F (43333/433/43)	0.1130	0.1597	−0.2726	11.27	0.17
5F (33333/333/33)	0.1624	0.2639	−0.4263	17.63	0.24
5F (43222/422/33)	0.1382	0.2448	−0.3829	15.84	0.28
5F (43333/433/43)	0.0936	0.1395	−0.2331	9.64	0.20
DFT(B3LYP)/6-311G**					
3F (33333/333/33)	0.2987	0.6140	−0.9127	37.74	0.35
3F (43222/422/33)	0.2725	0.5378	−0.8103	33.51	0.33
3F (43333/433/43)	0.1764	0.3042	−0.4806	19.87	0.27
5F (33333/333/33)	0.2849	0.5181	−0.8030	33.21	0.29
5F (43222/422/33)	0.2531	0.4341	−0.6872	28.42	0.26
5F (43333/433/43)	0.1458	0.2122	−0.3580	14.81	0.19

[a] Presented data are for calculations using 3F/5F basis sets on zirconium and 6-31G**/6-311G** for all other atoms. See the Experimental Section for details. [b] V_{ii} are principal components of the EFG tensor, where $|V_{33}| \geq |V_{22}| \geq |V_{11}|$. [c] Calculated EFG tensors were converted from atomic units (au) to megahertz by multiplying the largest component of the EFG tensor, V_{33}, by $eQ/h \times 9.71736 \times 10^{21}$ V m^{-2}, where $Q(^{91}Zr) = -1.76(3) \times 10^{-29}$ m^2,[1] and $e = 1.602188 \times 10^{-19}$ C.

Theoretical ^{91}Zr EFG tensors for Cp_2ZrCl_2 are presented in Table 3. In stark contrast to the calculated chemical shielding tensors, the majority of ab initio and hybrid DFT calculations overestimate the magnitude of the quadrupolar coupling constant (as do the EFG tensor calculations of Buhl et al.),[11] though better agreement with experimental data is seen for the EFG tensor asymmetry parameter $\eta_Q = 0.3(1)$. In particular, upon employing larger basis sets (3F3 and 5F3) on zirconium, correlation between theoretical and experimental ($C_Q = 6.35(10)$ MHz) zirconium quadrupole coupling constants improves, whereas values for η_Q stay in close agreement for all cases. The opposite is seen when a larger basis set (6-311G**) is used for Cl, C, and H atoms: C_Q values are larger and further away from the experimental values compared to values calculated with the smaller basis set (6-31G**). Notably, calculations employing zirconium F3 basis sets invariably result in better agreement with experimental values regardless of the calculation method employed, in agreement with observations gathered from the calculation of ^{91}Zr chemical shielding. For the case of Cp_2ZrCl_2, the zirconium 5F3 basis set gives the best results and RHF calculations are superior for predicting zirconium EFG parameters.

Experimental powder pattern simulations yield a ^{91}Zr CS tensor asymmetry parameter $\kappa = -0.55$ indicating that σ_{22} and σ_{33} are relatively similar in magnitude compared to σ_{11}, which is in good agreement with theory. Thus, σ_{11} should be oriented in a direction of distinct electronic environment compared to

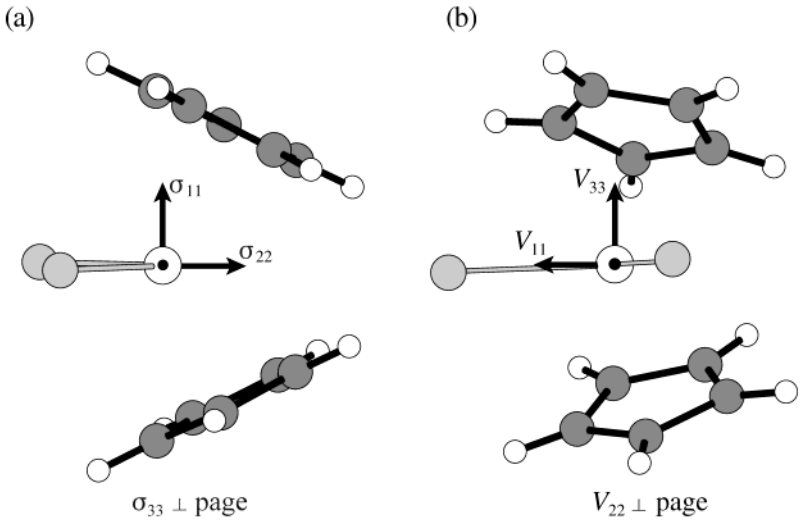

Figure 7. (a) Orientation of the zirconium CS tensor with respect to the theoretical ^{91}Zr EFG tensor given by the experimentally obtained Euler angles. (b) ^{91}Zr EFG tensor orientation within the molecular frame from calculations yielding the best agreement with experimental values.

σ_{22} and σ_{33}. Ab initio calculations (B3LYP/{6-31G**(Cl,C,H)|-5F3(Zr)}) resulting in the best agreement with experimental data predict a zirconium CS tensor where σ_{11} is oriented perpendicular to the plane formed by zirconium and the two chlorine atoms (hereafter referred to as the Cl−Zr−Cl plane), σ_{22} approximately bisects the Cl−Zr−Cl angle, and σ_{33} lies in the Cl−Zr−Cl plane, making a σ_{33}−Zr−Cl angle of about 37° with the nearest chlorine atom. With the exception of RHF calculations using basis sets {6-31G**|3F2}, {6-311G**|3F1}, and {6-311G**|3F2}, all remaining calculations (RHF and B3LYP) yield the ^{91}Zr CS tensor orientation described above.

Experimental powder pattern simulations reveal a nearly axial ^{91}Zr EFG tensor ($\eta_Q = 0.3(1)$) indicating that V_{11} and V_{22} are similar in magnitude; accordingly, V_{11} and V_{22} must be oriented in directions of similar electronic environments (i.e., similar electric field gradients). Although most theoretical values of the ^{91}Zr nuclear quadrupole coupling constant are not in agreement with the experimental C_Q of 6.35(10) MHz, all calculations yield very similar zirconium EFG tensor orientations. ^{91}Zr EFG tensors are calculated to have V_{33} oriented approximately perpendicular to the Cl−Zr−Cl plane (invariant across calculations). For the calculation which results in the best agreement between theoretical and experimental EFG tensor parameters (RHF/{6-31G**(Cl,C,H)|5F3(Zr)}), V_{11} and V_{22} lie approximately in the Cl−Zr−Cl plane (Cl−Zr−Cl angle 97°), making V_{ii}−Zr−Cl angles with the nearest chlorine atoms of approximately 13° and 19°, respectively (Figure 7b). All other calculations orient the zirconium EFG tensor in a similar fashion differing only slightly in the V_{11}−Zr−Cl (range +13° to −45°) and V_{22}−Zr−Cl (range +19° to −39°) angles. Following the conventions set out earlier, the ^{91}Zr EFG tensor is taken as the reference frame to deduce the orientation of the experimental CS tensor. The experimental zirconium CS tensor defined by Euler angles $\alpha = 26(5)°$, $\beta = 92(3)°$, and $\gamma = 10(1)°$ (Figure 7a) directs σ_{11}, σ_{22}, and σ_{33} in the same general directions as in the theoretically determined CS tensor, displaying only very slight deviations (Euler angles determined from theoretical calculations: $\alpha = 24.55°$, $\beta = 96.25°$, and $\gamma = 0.43°$). The remarkable agreement between the theoretical and experimental Euler angles ascertains the reliability of the CS and EFG tensor orientations determined herein. However, to unambiguously determine the orientation of the NMR interaction tensors with respect to the molecular frame, ^{91}Zr single-crystal NMR experiments on Cp_2ZrCl_2 would have to be performed. Much difficulty remains in producing accurate theoretical EFG parameters, which can be remedied in part by employing extended all-electron basis sets as seen for calculations with the 3F3 and 5F3 Zr basis sets. However, much work still remains in determining the optimal method and basis sets for calculation of ^{91}Zr NMR properties.

Conclusion

The use of recently developed signal-enhancement schemes, such as DFS/QCPMG, RAPT/QCPMG, and piecewise wideline QCPMG, for the acquisition of ^{91}Zr NMR spectra permits the study of an organometallic system with a moderate quadrupolar interaction, Cp_2ZrCl_2, as well as an inorganic material with a large quadrupolar interaction, a ceramic zirconium oxide NMR rotor. Experiments on samples contained within ceramic zirconium oxide rotors (the most common type of NMR rotor material available) indicate that static NMR experiments should be conducted with sample containers comprised of other materials due to the background ^{91}Zr rotor signal. On the other hand, MAS NMR experiments, which can only be conducted on samples with small to moderate values of $C_Q(^{91}Zr)$, are still feasible (background interference is minimal if the central transition signal is narrow enough to perform MAS NMR experiments). The performance of the RAPT/QCPMG and DFS/QCPMG pulse sequences on ^{91}Zr nuclei is investigated. It is demonstrated that a signal enhancement of an order of magnitude or more compared to the conventional spin echo can be attained, which can greatly facilitate the study of Zr-containing inorganic and organometallic compounds. We believe such techniques will be invaluable for the investigation of Zr-containing compounds important in heterogeneous and homogeneous catalysis, as well as countless other materials containing other unreceptive non-integer quadrupolar nuclei.

The anisotropic chemical shielding and quadrupolar interactions of the zirconium atom in Cp_2ZrCl_2 have been characterized by ^{91}Zr solid-state NMR experiments and ab initio calculations of NMR interaction tensors. Analytical and numerical powder line shape simulations reveal the first reported experimental evidence for ^{91}Zr chemical shielding anisotropy. Theoretical zirconium chemical shielding and electric field gradient tensors from RHF and hybrid DFT (B3LYP) calculations are in reasonable agreement with experimental values, with the best agreement between theory and experiment arising for calcula-

tions which use large basis sets (3F3 and 5F3) for zirconium and a relatively small basis set (6-31G**) on all other atoms. Experimental ^{91}Zr CS and EFG tensor orientations are elucidated from theoretical calculations and found to relate consistently with experimentally obtained data on relative tensor orientations. Further experimental determinations of NMR interaction tensors and corresponding ab initio calculations are clearly necessary to determine which theoretical methods and basis sets are appropriate for conducting calculations on zirconium-containing organometallic complexes.

Acknowledgment. We gratefully acknowledge Prof. Doug Stephan for use of his gloveboxes and Mr. Mike Fuerth for help using the Bruker DRX-500 NMR spectrometer. We would also like to thank Mr. Cory M. Widdifield for his help in determining the Euler angles between tensor orientations. This research was funded by Imperial Oil and the Natural Sciences and Engineering Research Council (NSERC—Canada). R.W.S. is also grateful to the Canadian Foundation for Innovation (CFI), the Ontario Innovation Trust (OIT), and the University of Windsor for funding the Solid-State NMR Facility at the University of Windsor. I.H. thanks the Centre for Catalysis and Materials Research (CCMR) at the University of Windsor for a graduate research scholarship.

Supporting Information Available: Listings of the SCF energy for all calculations, calculation results for the fully optimized structure as well as the second crystallographic site of Cp_2ZrCl_2, and comparison of wide-line spectra from addition and skyline projection of the subspectra of ZrO_2 (PDF). This material is available free of charge via the Internet at http://pubs.acs.org.

References and Notes

(1) Kello, V.; Pyykko, P.; Sadlej, A. J.; Schwerdtfeger, P.; Thyssen, J. *Chem. Phys. Lett.* **2000**, *318*, 222.
(2) Yamada, Y.; Ohira, K. *J. Phys. Soc. Jpn.* **1983**, *52*, 3646.
(3) Bastow, T. J. *J. Phys.: Condens. Matter* **1990**, *2*, 6327.
(4) Fitzgerald, J. J.; Han, S. S.; Dec, S. F.; Davis, M. F.; Bronnimann, C. E.; Maciel, G. E. *NIST Spec. Publ.* **1991**, *804*, 173.
(5) Dec, S. F.; Davis, M. F.; Maciel, G. E.; Bronnimann, C. E.; Fitzgerald, J. J.; Han, S. S. *Inorg. Chem.* **1993**, *32*, 955.
(6) Hartman, J. S.; Koffyberg, F. P.; Ripmeester, J. A. *J. Magn. Reson.* **1991**, *91*, 400.
(7) Bastow, T. J.; Hobday, M. E.; Smith, M. E.; Whitfield, H. J. *Solid State Nucl. Magn. Reson.* **1994**, *3*, 49.
(8) Bastow, T. J.; Hobday, M. E.; Smith, M. E.; Whitfield, H. J. *Solid State Nucl. Magn. Reson.* **1996**, *5*, 293.
(9) Bastow, T. J.; Forwood, C. T.; Gibson, M. A.; Smith, M. E. *Phys. Rev. B* **1998**, *58*, 2988.
(10) Benn, R.; Rufinska, A. *J. Organomet. Chem.* **1984**, *273*, C51.
(11) Buhl, M.; Hopp, G.; von Philipsborn, W.; Beck, S.; Prosenc, M. H.; Rief, U.; Brintzinger, H. H. *Organometallics* **1996**, *15*, 778.
(12) Janiak, C.; Lange, K. C. H.; Versteeg, U.; Lentz, D.; Budzelaar, P. H. M. *Chem. Ber./Recl.* **1996**, *129*, 1517.
(13) Kunwar, A. C.; Turner, G. L.; Oldfield, E. *J. Magn. Reson.* **1986**, *69*, 124.
(14) Bastow, T. J.; Smith, M. E.; Stuart, S. N. *Chem. Phys. Lett.* **1992**, *191*, 125.
(15) Hartmann, P.; Scheler, G. *Z. Naturforsch., A* **1995**, *50*, 90.
(16) Lipton, A. S.; Sears, J. A.; Ellis, P. D. *J. Magn. Reson.* **2001**, *151*, 48.
(17) Smith, M. E. *Annu. Rep. NMR Spectrosc.* **2001**, *43*, 121−175.
(18) Larsen, F. H.; Jakobsen, H. J.; Ellis, P. D.; Nielsen, N. C. *J. Phys. Chem. A* **1997**, *101*, 8597.
(19) Larsen, F. H.; Skibsted, J.; Jakobsen, H. J.; Nielsen, N. C. *J. Am. Chem. Soc.* **2000**, *122*, 7080.
(20) Larsen, F. H.; Lipton, A. S.; Jakobsen, H. J.; Nielsen, N. C.; Ellis, P. D. *J. Am. Chem. Soc.* **1999**, *121*, 3783.
(21) Lipton, A. S.; Buchko, G. W.; Sears, J. A.; Kennedy, M. A.; Ellis, P. D. *J. Am. Chem. Soc.* **2001**, *123*, 992.
(22) Larsen, F. H.; Jakobsen, H. J.; Ellis, P. D.; Nielsen, N. C. *J. Magn. Reson.* **1998**, *131*, 144.
(23) Larsen, F. H.; Nielsen, N. C. *J. Phys. Chem. A* **1999**, *103*, 10825.
(24) Yao, Z.; Kwak, H. T.; Sakellariou, D.; Emsley, L.; Grandinetti, P. J. *Chem. Phys. Lett.* **2000**, *327*, 85.
(25) Kentgens, A. P. M.; Verhagen, R. *Chem. Phys. Lett.* **1999**, *300*, 435.
(26) Schurko, R. W.; Hung, I.; Widdifield, C. M. *Chem. Phys. Lett.* **2003**, *379*, 1.
(27) Mortara, S.; Fregonese, D.; Bresadola, S.; Boaretto, R.; Sostero, S. *J. Polym. Sci., Polym. Chem.* **2001**, *39*, 4243.
(28) Van Veenendaal, E.; Meier, B. H.; Kentgens, A. P. M. *Mol. Phys.* **1998**, *93*, 195.
(29) Medek, A.; Frydman, V.; Frydman, L. *J. Phys. Chem. A* **1999**, *103*, 4830.
(30) Bryant, P. L.; Butler, L. G.; Reyes, A. P.; Kuhns, P. *Solid State Nucl. Magn. Reson.* **2000**, *16*, 63.
(31) Schurko, R. W.; Wi, S.; Frydman, L. *J. Phys. Chem. A* **2002**, *106*, 51.
(32) Madhu, P. K.; Pike, K. J.; Dupree, R.; Levitt, M. H.; Smith, M. E. *Chem. Phys. Lett.* **2003**, *367*, 150.
(33) Bak, M.; Rasmussen, J. T.; Nielsen, N. C. *J. Magn. Reson.* **2000**, *147*, 296.
(34) Mehring, M. *Principles of High-Resolution NMR in Solids*; Springer-Verlag: New York, 1983.
(35) Zare, R. N. *Angular Momentum: Understanding Spatial Aspects in Chemistry and Physics*; John Wiley & Sons: Toronto, 1988.
(36) Frisch, M. J.; Trucks, G. W.; Schlegel, H. B.; Scuseria, G. E.; Robb, M. A.; Cheeseman, J. R.; Zakrzewski, V. G.; Montgomery, J., J. A.; Stratmann, R. E.; Burant, J. C.; Dapprich, S.; Millam, J. M.; Daniels, A. D.; Kudin, K. N.; Strain, M. C.; Farkas, O.; Tomasi, J.; Barone, V.; Cossi, M.; Cammi, R.; Mennucci, B.; Pomelli, C.; Adamo, C.; Clifford, S.; Ochterski, J.; Petersson, G. A.; Ayala, P. Y.; Cui, Q.; Morokuma, K.; Malick, D. K.; Rabuck, A. D.; Raghavachari, K.; Foresman, J. B.; Cioslowski, J.; Ortiz, J. V.; Baboul, A. G.; Stefanov, B. B.; Liu, G.; Liashenko, A.; Piskorz, P.; Komaromi, I.; Gomperts, R.; Martin, R. L.; Fox, D. J.; Keith, T.; Al-Laham, M. A.; Peng, C. Y.; Nanayakkara, A.; Challacombe, M.; Gill, P. M. W.; Johnson, B.; Chen, W.; Wong, M. W.; Andres, J. L.; Gonzalez, C.; Head-Gordon, M.; Replogle, E. S.; Pople, J. A. *Gaussian 98*, revision A.9; Gaussian, Inc.: Pittsburgh, PA, 1998.
(37) Repo, T.; Klinga, M.; Mutikainen, L.; Su, Y.; Leskela, M.; Polamo, M. *Acta Chem. Scand.* **1996**, *50*, 1116.
(38) Becke, A. D. *Phys. Rev. A* **1988**, *38*, 3098.
(39) Becke, A. D. *J. Chem. Phys.* **1993**, *98*, 5648.
(40) Lee, C.; Yang, W.; Parr, R. G. *Phys. Rev. B* **1988**, *37*, 785.
(41) Huzinaga, S., Ed. *Gaussian Basis Sets for Molecular Calculations*; Elsevier: New York, 1984.
(42) Ditchfield, R. *Mol. Phys.* **1974**, *27*, 789.
(43) Wolinski, K.; Hinton, J. F.; Pulay, P. *J. Am. Chem. Soc.* **1990**, *112*, 8251.
(44) Lipton, A. S.; Wright, T. A.; Bowman, M. K.; Reger, D. L.; Ellis, P. D. *J. Am. Chem. Soc.* **2002**, *124*, 5850.
(45) Baugher, J. F.; Taylor, P. C.; Oja, T.; Bray, P. J. *J. Chem. Phys.* **1969**, *50*, 4914.
(46) Power, W. P.; Wasylishen, R. E.; Mooibroek, S.; Pettitt, B. A.; Danchura, W. *J. Phys. Chem.* **1990**, *94*, 591.
(47) Cheng, J. T.; Edwards, J. C.; Ellis, P. D. *J. Phys. Chem.* **1990**, *94*, 553.
(48) Haase, J.; Conradi, M. S. *Chem. Phys. Lett.* **1993**, *209*, 287.
(49) Madhu, P. K.; Goldbourt, A.; Frydman, L.; Vega, S. *Chem. Phys. Lett.* **1999**, *307*, 41.
(50) Iuga, D.; Schafer, H.; Verhagen, R.; Kentgens, A. P. M. *J. Magn. Reson.* **2000**, *147*, 192.